HHS Public Access

Author manuscript

Cancer Res. Author manuscript; available in PMC 2018 January 01.

Published in final edited form as:

Cancer Res. 2017 July 01; 77(13): 3513–3526. doi:10.1158/0008-5472.CAN-16-3424.

Inhibition of mitochondrial matrix chaperones and anti-apoptotic Bcl-2 family proteins empower antitumor therapeutic responses

Georg Karpel-Massler[1], **Chiaki Tsuge Ishida**[1], **Elena Bianchetti**[1], **Chang Shu**[1], **Rolando Perez-Lorenzo**[2], **Basil Horst**[1,2], **Matei Banu**[3], **Kevin A. Roth**[1], **Jeffrey N. Bruce**[3], **Peter Canoll**[1], **Dario C. Altieri**[4], and **Markus D. Siegelin**[1]

[1]Department of Pathology & Cell Biology, Columbia University Medical Center, New York, New York, U.S.A

[2]Department of Dermatology, Columbia University Medical Center, New York, New York, U.S.A

[3]Department of Neurosurgery, Columbia University Medical Center, New York, New York, U.S.A

[4]The Wistar Institute, Philadelphia, Pennsylvania, U.S.A

Abstract

Rational therapeutic approaches based on synthetic lethality may improve cancer management. Based on a high-throughput drug screen, we provide preclinical proof of concept that targeting the mitochondrial Hsp90 chaperone network (mtHsp90) and inhibition of Bcl-2, Bcl-xL and Mcl-1 is sufficient to elicit synthetic lethality in tumors recalcitrant to therapy. Our analyses focused on BH3 mimetics that are broad acting (ABT263 and Obatoclax) or selective (ABT199, WEHI-539 and A1210477), along with the established mitochondrial matrix chaperone inhibitor Gamitrinib-TPP. Drug combinations were tested in various therapy-resistant tumors in vitro and in vivo in murine model systems of melanoma, triple-negative breast cancer and patient-derived orthotopic xenografts of human glioblastoma (PDX). We found that combining BH3-mimetics and Gamitrinib-TPP blunted cellular proliferation in a synergistic manner by massive activation of intrinsic apoptosis. In like manner, suppressing either Bcl-2, Bcl-xL or Mcl-1 recapitulated the effects of BH3-mimetics and enhanced the effects of Gamitrinib-TPP. Mechanistic investigations revealed that Gamitrinib-TPP activated a PERK-dependent integrated stress response which activated the pro-apoptotic BH3 protein Noxa and its downstream targets Usp9X and Mcl-1. Notably, in the PDX glioblastoma and BRAFi-resistant melanoma models, this drug combination safely and significantly extended host survival. Our results show how combining mitochondrial chaperone and Bcl-2 family inhibitors can synergize to safely degrade the growth of tumors recalcitrant to other treatments.

Correspondence to: Markus D. Siegelin, MD, Dr. med., Department of Pathology & Cell Biology, Columbia University Medical Center, 630 West 168th Street, P&S Rm. 15-415, New York, NY 10032, Phone: 212 305 1993, ms4169@cumc.columbia.edu, msiegelin@gmail.com.

Conflict of interest statement: The authors have declared that no conflict of interest exists.

Introduction

Mitochondrial heat shock protein-90 (mtHsp90) has been shown to be of utmost importance for cancer cell survival and growth (1). Gamitrinib-triphenylphosphonium (G-TPP) is a synthetic small molecule Hsp90 ATPase antagonist with preferential tropism to mitochondria (2). In preclinical studies, G-TPP was shown to have inhibitory effects on various pro-neoplastic features in different cancer types (2–8).

The anti-apoptotic Bcl-2 family members regulate cell death at the outer mitochondrial membrane (9–14). Since Bcl-2 and Bcl-xL are frequently increased in cancer cells and bear a major inhibitory impact on apoptosis, a novel class of pro-apoptotic compounds, called BH3-mimetics, such as ABT263 or ABT199 (15,16), was developed. However, they fail to inhibit Mcl-1. Therefore, strategies need to be tailored that lower Mcl-1 levels in tumor cells.

In this report, we demonstrate that Gamitrinib decreases protein levels of both Mcl-1 and its deubiquitinase Usp9X by activation of the integrated stress response. Consequently, we tested the hypothesis that interference with mitochondrial matrix chaperone proteins combined with inhibition of anti-apoptotic Bcl-2 family members would facilitate cancer cell death as a consequence of a pro-apoptotic mitochondria-specific “dual-hit”. This hypothesis was supported by an ealier drug screen that demonstrated that BH3-mimetics and Gamitrinib are potentially synergistic (7). Our data show that disruption of the Hsp90 chaperone network when combined with BH3-mimetics yields a synergistic anti-proliferative and pro-apoptotic effect across a wide panel of different cancer cells. Moreover, combined treatment with the mitochondrial chaperone inhibitor G-TPP and BH-3 mimetics results in a significant enhancement of tumor growth inhibition in several *in vivo* model systems, including patient-derived xenografts.

Materials and Methods

Reagents

ABT263, GX15-070, ABT199, WEHI-539 and A-1210477 were purchased from Selleckchem (Houston, TX). G-TPP was synthesized as described earlier (4).

Cell cultures and growth conditions

U87MG, LN229, U251 and T98G human glioblastoma cell lines and Colo-829 and MeWo were obtained from the American Type Culture Collection (Manassas, VA). WC62 melanoma cells were from Coriell Cell Repositories, Camden, NJ. NCH644 and NCH421K stem cell-like glioma cells were obtained from Cell Line Services (CLS, Heidelberg, Germany). The respective cell line depository authenticated the cells. U87-EGFRvIII cells were kindly provided by Dr. Frank Furnari (Ludwig Institute for Cancer Research, La Jolla, CA). The GS9-6 (17) are primary neurosphere stem-like glioma cells derived at the University of Massachusetts (Worcester, MA). All cell lines were obtained between 2013–2015. The MGPP-3 (p53−/−, PTEN+/+, PDGFR+) are murine proneural glioblastoma cells. All cells were cultured as previously described (12,18–21).

Cell viability assays

In order to examine cellular proliferation, 3-[4, 5-dimethylthiazol-2-yl]-2, 5-diphenyltetrazolium bromide (MTT) assays were performed as previously described (18,22,23).

Measurement of apoptosis and mitochondrial membrane potential

For Annexin V/propidium iodide staining the Annexin V Apoptosis Detection Kit (BD Pharmingen) was used as previously described (24,25). For PI staining, cells were resuspended in 300 μl PBS and fixated by adding 1000 μl ice-cold ethanol prior to incubation over night at 4°C. Then the cells were centrifuged at 1800 rpm, the supernatant was removed and 400 μl PI/RNase staining solution (Cell signaling technology, Danvers, MA) were added prior to incubation for 15 min at RT and flow cytometric analysis. To detect intrinsic apoptosis staining and loss of mitochondrial membrane potential, TMRE staining was performed according to the manufacturer's instructions (Mitochondrial Membrane Potential kit, Cell Signaling Technology, Danvers, MA). The data were analyzed with the FlowJo software (version 8.7.1; Tree Star, Ashland, OR).

Transfections of siRNAs

Briefly, cells were incubated for 6h with the formed complexes of Oligofectamine® 2000 (Invitrogen, Carlsbad, CA) and the respective siRNA (12-well condition) in DMEM without FBS and antibiotics. After 6h, FBS was added to a total concentration of 1.5%.

Western blot analysis

Specific protein expression in cell lines was determined by Western blot analysis as described before (26).

Orthotopic patient-derived xenograft glioma model

Patient-derived xenograft cells were stereotactically injected into 6–8 week-old male or female nude GFP or SCID SHO mice as previously described (22,24). A burr hole was positioned 2mm anterior and 2mm lateral of the bregma prior to introducing a Hamilton syringe under stereotactic guidance 3mm into the striatum. Motorized injections of the cells were performed at a rate of 0.5μL/min. MRI imaging was performed using a Bruker BioSpec™, 9.4 Tesla imaging device. Survival was assessed by calculating Kaplan–Meier curves.

Subcutaneous xenograft model

1×10^6 U251, LN229, U87MG, A375 or A375R cells were implanted subcutaneously into the flanks of 6–8 week-old SCID SHO mice as described before (22,24). Measurements were performed with a caliper and tumor sizes were calculated as (length × width^2)/2. Treatment was performed intraperitoneally twice a week for 3 weeks. For intraperitoneal application G-TPP, ABT263 and GX15-070 were dissolved in 80% Cremophor EL (SIGMA, St. Louis, MO) and 20% Ethanol (Pharmco-Aaper, Brookfield,CT) (v/v).

Statistical analysis

Statistical significance was assessed by Student's t-test using Prism version 7.00 (GraphPad, La Jolla, CA). A $p \leq 0.05$ was considered statistically significant. Bliss analysis was performed to detect synergistic, additive or antagonistic effects as previously described (20).

Study approval

All procedures were in accordance with Animal Welfare Regulations and approved by the Institutional Animal Care and Use Committee at the Columbia University Medical Center.

Results

Inhibition of mitochondrial chaperones primes tumor cells for apoptosis by broad and selective BH3–mimetics

To assess whether inhibition of mitochondrial Hsp90 chaperones primes tumor cells to apoptosis, a broad range of tumor cells were analyzed by MTT assay for viability after treatment with ABT263, GX15-070, G-TPP or the indicated combination treatments (Figure 1A). In U87MG, LN229, U251 and T98G established glioblastoma cells as well as in GS9-6 and NCH644 stem cell-like glioma cells, GBM6, GBM39 patient–derived xenograft glioblastoma cells and in primary proneural murine glioblastoma cells (MGPP-3, derived from a transgenic model) a synergistic reduction in cellular viability was found when cells were treated with the combination of ABT263 and G-TPP (Figure 1B,C, Suppl. fig. 1 and 2, Suppl. tables 1 and 2). In contrast, U87-EGFRvIII cells treated with the combination therapy of ABT263 and G-TPP showed only an additive effect (Figure 1B and Suppl. table 1). Next, we assessed whether these observations are restricted to glioblastoma cells. Similarly, BRAF-mutated melanoma cells, A375, BRAF-inhibitor resistant, A375R, WC62, MeWo and COLO 829 melanoma cells as well as triple receptor-negative breast cancer cells, MDA-MB-468, displayed a synergistic reduction in viability after treatment with ABT263 and G-TPP (Figure 1B, Suppl. fig. 3, Suppl. tables 1 and 3). While the combination treatment did not yield a synergistic anti-proliferative effect on pancreatic cancer cells, PANC1, the combination treatment revealed at least enhanced anti-proliferative activity when compared to treatment with each compound alone (Suppl. fig. 3, Suppl. table 1). Akin to ABT263, GX15-070 broadly enhanced apoptosis and loss of cellular viability induced by mitochondrial matrix inhibitors in a synergistic manner (Figure 1B,D, Suppl. fig. 1 and 7, Suppl. table 1). Given that ABT263 and GX15-070 are broad BH3-mimetics, we assessed as to whether selective BH3-mimetics would synergize with G-TPP as well. To this end, U87MG and T98G cells were treated with the selective Bcl-xL inhibitor WEHI-539, the selective Bcl-2 inhibitor ABT199 and the selective Mcl-1 inhibitor A-1210477 in the presence or absence of G-TPP. Our data show that G-TPP combined with each of these BH3-mimetics caused a synergistic reduction in cellular viability (Figure 1E,F, Suppl. table 4). Similar results were achieved in LN229 and GBM6 cells (Suppl. table 4), suggesting that G-TPP primes mitochondria for broad and selective BH3-mimetics and that likely this involves in part the mitochondriotoxic properties of G-TPP. Combined treatment with ABT263 and G-TPP displayed typical features of apoptosis, such as enhanced cellular fragmentation and blebbing (Figure 1G). In U87MG, U87-EGFRvIII, T98G and LN229 glioblastoma cell lines enhanced DNA fragmentation was detected in cells treated with the

combination of ABT263 and G-TPP (Suppl. fig. 4A). U87-EGFRvIII cells were least responsive. It should be noted that strongest synergy in cell proliferation assays correlated with the most prominent DNA fragmentation/apoptosis. To further verify whether apoptosis induction is a relevant part of the mechanism, we performed Annexin V/Propidium iodide staining in U87MG and T98G cells (Figure 2A). Combined treatment with ABT263 and G-TPP resulted in a significant induction of apoptotic cell death as compared to either treatment alone. Consistently, both U87MG and T98G cells treated with ABT263/G-TPP displayed enhanced reduction of the mitochondrial membrane potential when compared to cells treated with each compound alone (Figure 2B). T98G and LN229 cells exposed to the combination treatment revealed enhanced cleavage of both caspase-9 and caspase-3 (Figure 2C). Furthermore, pan-caspase inhibition abolished the pro-apoptotic response following a combined treatment with ABT263 and G-TPP (Figure 2D). In contrast, treatment with Necrostatin, a necroptosis inhibitor, did not affect apoptosis driven by the combination therapy which supports a caspase-mediated specific apoptotic response as mechanism (Figure 2E). Next, we assessed to what extent selective BH3-mimetics induced apoptosis and mediated loss of the mitochondrial membrane potential in the presence or absence of G-TPP. U251, T98G, LN229 and U87MG established glioblastoma cells, NCH644 glioma stem cell-like cells as well as MeWo and WC62 melanoma cells were treated with the selective BH3-mimetics, WEHI-539, ABT199 and A-1210477 alone and in combination with G-TPP. We found that G-TPP enhanced apoptosis for all selective BH3-mimetics (Figure 2F,G, Suppl. fig. 4B, Suppl. fig. 5). Similar findings were made with regards to loss of the mitochondrial membrane potential in WC62, MeWo and T98G cells (Suppl. fig. 6). In order to confirm the above findings with selective BH3-mimetics, we silenced the expression of Bcl-xL, Bcl-2 or Mcl-1 in LN229 glioblastoma cells (Figure 3A,B). Our data show that cells silenced for Bcl-xL, Bcl-2 or Mcl-1 combined with G-TPP treatment displayed a significantly enhanced fraction of sub-G1 cells, which recapitulates our findings with the selective BH3-mimetics we reported above (Figure 3A). Concerning the relative contribution of each anti-apoptotic Bcl-2 family member, it appears that this is cell type-dependent.

To account for the role of Bax and Bak in ABT263/G-TPP-mediated cell death, we perfomed double-knockdown experiments for Bax and Bak. As shown in Figure 3C, Bax/Bak-silenced LN229 cells treated with ABT263/G-TPP showed a marked reduction in the fraction of Annexin V-positive cells when compared to cells treated with n.t.-siRNA instead. For single-agent treatments, only minor effects were noted in the presence of Bax/Bak knockdown when compared to treatment with n.t.-siRNA. In line with this finding, dual Bax/Bak knockdown resulted in reduced cleavage of PARP and caspase-3 in cells treated with ABT263/G-TPP (Figure 3D). For further clarification of the role of Bax in this setting, we conducted an immunoprecipitation for active Bax and found that ABT263, G-TPP and the combination of both resulted in an activation of Bax, suggesting that Bax might be required for cell death execution, but that it is not solely responsible for it (Figure 3E). To demonstrate that pro-apoptotic molecules are released upon treatment with the drug combination of ABT263 and G-TPP, LN229 cells were treated with ABT263, G-TPP or the combination of both for 7h. Lysates were prepared and immunoprecipitated with an antibody against Mcl-1 (Figure 3G,H). Immunoblots for BIM protein indicate that Mcl-1 avidly binds BIM protein in untreated LN229 cells. Notably, LN229 cells that were treated with ABT263

revealed increased binding of BIM to Mcl-1, suggesting that Mcl-1 counteracts the pro-apoptotic effect of Bcl-2/Bcl-xL inhibition by absorbing BIM protein. The combination treatment of ABT263 and G-TPP resulted in a release of BIM from Mcl-1, thereby facilitating intrinsic apoptosis. Moreover, specific silencing of BIM by siRNA attenuates caspase-3 cleavage induced by the combination treatment of ABT263 and G-TPP, further supporting the role of BIM in ABT263/G-TPP-mediated cell death (Figure 3F).

Mitochondrial matrix inhibitors cause a depletion of Mcl-1 and its interacting deubiquitinase, Usp9X

Expression of Mcl-1 is a mechanism of resistance towards ABT199, ABT263 and ABT737. We therefore focused our next studies on determining effects of G-TPP on expression of Mcl-1. As shown in Figure 4A, protein levels of Mcl-1 were decreased in LN229, U251, A375 and HL-60 cells following treatment with G-TPP in a dose-dependent manner. Consistent with this finding, expression of the deubiquitinating enzyme Usp9X was also markedly decreased. Notably, real-time rtPCR analyses suggest that down-regulation of both Mcl-1 and Usp9X is not mediated on the transcriptional level (Suppl. fig. 8A,B). In contrast, both protein and mRNA levels of Noxa, a known pro-apoptotic interactor of Mcl-1, were consistently increased (Suppl. fig. 8C). Given our observation that Mcl-1 and Usp9X are suppressed by G-TPP, we determined as to whether Mcl-1 or Usp9X levels determine the sensitivity of cancer cells towards the BH3-mimetic, ABT263. To this end, we knocked down Mcl-1 (Figure 4B,C, Suppl. fig. 9A–D) and Usp9X (Figure 4D,E, Suppl. fig. 9E–H) by siRNA and observed that both Mcl-1 and Usp9X knockdown potently sensitized LN229 and U251 glioblastoma cells as well as A375 melanoma cells to the cytotoxic effects of ABT263, indicating that Mcl-1 and Usp9X levels are key regulators in ABT263-mediated apoptosis. Next, we assessed whether the G-TPP-mediated reduction in Mcl-1 and Usp9X protein is posttranslationally driven. LN229 cells were treated with the protein synthesis inhibitor cycloheximide in the presence or absence of G-TPP. The protein stability of both Mcl-1 and its interacting deubiquitinase Usp9X was significantly decreased in the presence of a mitochondrial matrix inhibitor. This suggests that G-TPP suppresses Mcl-1 and Usp9X levels in a posttranslational manner (Figure 4F). Furthermore, inhibition of proteasomal degradation using MG-132 lead to a rescue of Usp9X and Mcl-1 levels (Figure 4G). Western blot analyses showed that treatment with G-TPP results in enhanced protein expression of Noxa, a pro-apoptotic BH3-only Bcl-2 family member, which is known to interact with Mcl-1. We therefore examined next whether Noxa is implicated in G-TPP/ABT263-mediated cell death (Figure 4H). LN229 glioblastoma cells were transfected with a non-targeting siRNA or two different Noxa-specific siRNAs (Figure 4H,I). LN229 cells treated with the combination therapy showed a marked reduction of the fraction of sub-G1 cells in the presence of Noxa knockdown. To assess whether the up regulation of Noxa also results in an increased binding of Noxa to Mcl-1 we performed co-immunoprecipitation experiments (Figure 4J). LN229 glioblastoma cells were treated with ABT263, G-TPP or solvent. Subsequently, cells were immunoprecipitated with a monoclonal Mcl-1 antibody and analyzed for the expression of Mcl-1 and Noxa. While treatment with ABT263 barely affected the binding of Noxa to Mcl-1, treatment with G-TPP lead to a significant increase of the Noxa/Mcl-1 ratio.

G-TPP-mediated down regulation of Mcl-1 and Usp9X is Noxa-dependent

LN229 cells treated with increasing concentrations of G-TPP displayed a marked decrease in Mcl-1 and Usp9X levels (Figure 4K–M, Suppl. fig.10). However, in the presence of Noxa knockdown with two different siRNAs this effect was significantly attenuated (Figure 4K–M, Suppl. fig.10).

G-TPP treatment mediates an ER-stress response

Up-regulation of Noxa is a well-described downstream effect of an unfolded protein response. Previous microarray analyses indicated that low doses of G-TPP cause an unfolded protein response in U251 and LN229 cells, which was accompanied by a transcriptional increase in *PMAIP1*. In addition, earlier work suggested that interference with mitochondrial matrix chaperone elicits an increase of ER-stress proteins (27). To determine if a similar up-regulation in the unfolded protein response was occurring in our system, we performed Western blot analysis for typical ER-stress markers in LN229 cells treated with increasing concentrations of G-TPP. As shown in Figure 5A, G-TPP treatment elicits a distinct ER-stress signature, including up regulation of IRE1α, pPERK, CHOP, GRP78 and C/EBPB. On the transcriptional level, these findings were confirmed, showing upregulation of downstream cascade effectors (C/EBPB, XBP1, GRP78, ATF5 and CHOP) (Figure 5B, Suppl. fig. 8D). To further characterize the link between Noxa up-regulation and G-TPP-mediated ER stress we next examined effects of G-TPP on the integrated stress response. LN229 and U251 cells treated with increasing concentrations of G-TPP showed a dose-dependent increase in p-eIF2α levels, which coincided with a marked increase in ATF4 expression (Figure 5C,D). To further examine the causal relationship between ATF4 and Noxa levels, LN229 and U251 cells were transfected with a specific siRNA against ATF4. LN229 and U251 cells silenced for ATF4 showed an attenuated up-regulation of Noxa after treatment with G-TPP, suggesting that ATF4 plays a central role in G-TPP-mediated up-regulation of Noxa (Figure 5E,F). PERK (protein kinase R-like endoplasmic reticulum kinase) acts as one of the key sensors for the unfolded protein response and is known to activate eIF2α. To extend our understanding on the role of ER stress with respect to G-TPP-mediated ATF4 and Noxa up-regulation, we performed knockdown experiments. As we observed before treatment with G-TPP results in a marked up-regulation of ATF4 (Figure 5G–J). However, in the presence of PERK knockdown, using two different siRNAs ATF4 expression was suppressed despite simultaneous treatment with G-TPP.

The combination treatment of Gamitrinib and BH3-mimetics prolongs survival in an orthotopic glioma patient-derived xenograft model

We next examined whether a combined inhibition of mitochondrial matrix chaperones and Bcl-2/Bcl-xL yields enhanced therapeutic efficacy *in vivo*. To this purpose, GBM12 patient-derived xenograft cells were implanted into the right striatum of nude mice and allowed to form tumors prior to randomization into 4 treatment arms as outlined in Figure 6A. Animals bearing GBM12 tumors subjected to the combination therapy had significantly prolonged overall survival compared to animals receiving vehicle or single-agent treatments (median survival: control 21d, ABT263 32.5d, G-TPP 31d and ABT263+G-TPP 85d) (Figure 6A). In

line with this finding, GBM12 tumor size was markedly reduced in animals treated with the combination therapy as assessed by MRI imaging (Figure 6B).

Combined inhibition of mitochondrial matrix chaperones and Bcl-2/Bcl-xL reduces tumor growth rate in heterotopic glioma models

We further extended our *in vivo* studies onto multiple heterotopic glioma models. Mice carrying subcutaneous xenografts of LN229, U251 and U87MG glioma cells were randomized to the respective treatment groups and tumor sizes were measured (Figure 6C–H). In all models studied, the growth rate of tumors forming in mice that were subjected to treatment with the combination therapy was reduced. The mean tumor size of tumors that formed in animals subjected to the combination therapy was significantly reduced compared to vehicle or single-agent treatments (Figure 6C–H). Moreover, in all three models the combined treatment with G-TPP and ABT263 or G-TPP and GX15-070 yielded regression of tumors. Notably, histologic analyses with respect to potential toxic side effects of the combination therapy revealed no detectable noxious effects on solid organs (Suppl. fig. 11).

Combined inhibition of mitochondrial matrix chaperones and Bcl-2/Bcl-xL reduces the tumor growth rate in orthotopic breast cancer and melanoma models

For the breast cancer model, MDA-MB-231 cells were implanted into the mammary fat pad of nude mice. Toward the end of the experiment, the mean size of tumors developing in mice that received the combination therapy was significantly reduced compared to vehicle treated mice (Suppl. fig. 12). However, despite a clear trend, no statistically significant difference compared to the mean tumor size in the single-agent treatment groups was noted and no regression of tumors was achieved. For the melanoma model, A375 cells were implanted subcutaneously and treatment was initiated as indicated once tumors formed (Figure 7A–E). Animals subjected to the combination therapy showed a marked reduction of the tumor growth rate culminating in a significantly decreased mean tumor size towards the end of the experiment when compared to single treatments or vehicle (Figure 7A–C). Histological analysis revealed a marked decrease in Ki-67 staining (Figure 7D) and a marked increase in TUNEL staining (Figure 7E) in those tumors forming in animals that received the combination therapy suggesting that the anti-tumor effect of the combination therapy is not only due to inhibitory effects on proliferation, but also due to enhanced cell death induction. Treatment with B-Raf^{V600E} inhibitors represents a mainstay in the treatment of B-Raf^{V600E}-mutated melanomas. Unfortunately, development of resistance towards B-Raf^{V600E} inhibitors is a common event. Therefore, we examined whether the combination treatment with ABT263 and G-TPP would prove to be advantageous in a model of B-Raf^{V600E} inhibitor-resistant melanoma (A375R). *In vitro*, combined treatment with ABT263 and G-TPP yielded a synergistic anti-proliferative activity in A375R cells (Suppl. fig. 3B). To test whether this finding also holds up *in vivo*, A375R cells were implanted subcutaneously and tumors were allowed to form prior to treatment. Animals treated with the B-Raf^{V600E} inhibitor PLX-4720 displayed only a slight therapeutic response (Figure 7F–H). However, those animals subjected to treatment with the combination therapy in the presence or absence of PLX-4720 showed a significantly reduced tumor growth rate and mean tumor size toward the end of the experiment (Figure 7F–H).

Discussion

High levels of Mcl-1 are known to cause therapeutic resistance towards a certain class of BH3-mimetics (28), which only bind to Bcl-2, Bcl-xL and Bcl-w, but not Mcl-1 (10–14,29,30). Mcl-1 is an unstable protein and is regulated by the deubiquitinase Usp9X (31), which is increased in tumors as well, mediates therapeutic resistance and is explored as a potential drug target (22,31). Researchers have focused to develop strategies to suppress Mcl-1 levels by targeting the different regulatory levels of Mcl-1 expression (12,18,22,24–26,32–37). Other mechanisms for sensitization to BH3-mimetics include up-regulation of the pro-apoptotic BIM (38,39).

In this report, we have provided evidence that inhibition of mtHSP90 (2,6,18,40,41) by G-TPP leads to a reduction of Mcl-1 (42) and its partner Usp9X by eliciting an integrated stress response (ISR) dependent on ATF4 (43–45) with a subsequent increase in pro-apoptotic Noxa. In turn, Noxa destabilizes both Mcl-1 and Usp9X, sensitizing broadly to the cell death inducing effects of selective and broad BH3-mimetics. Others have described a similar relationship between Noxa and Usp9X after Pemetrexed treatment (46). This is the first report, demonstrating that mitochondrial matrix chaperones control the levels of anti-apoptotic Mcl-1. However, based on our results that selective inhibition of Mcl-1 by A-1210477 and siRNA enhances G-TPP-mediated cell death, it is likely that the general tumor-specific mitochondriotoxic properties of G-TPP contributed to the enhancement of BH3-mimetic-mediated cell death as well.

Our findings suggest that this treatment strategy is efficacious in a broad range of *in vivo* model system, is well tolerated and did not reveal any histologically detectable damages to major organ systems, consistent with earlier findings in vivo (5). Therefore, our proposed strategy of targeting Bcl-2 family proteins along with mitochondrial matrix chaperones warrants testing in clinical trials.

Supplementary Material

Refer to Web version on PubMed Central for supplementary material.

Acknowledgments

Financial Support:

G. Karpel-Massler: Scholarship from Dr. Mildred Scheel foundation of the German Cancer Aid.

D.C. Altieri: NIH NCI P01CA140043

M.D. Siegelin: NIH NINDS R01NS095848 and K08NS083732, 2013 AACR-National Brain Tumor Society Career Development Award for Translational Brain Tumor Research (13-20-23-SIEG), BCURED Fighting Brain Cancer Award (16-0992), American Brain Tumor Association, Translational Grant 2013 (ABTACU13-0098)

References

1. Chae YC, Caino MC, Lisanti S, Ghosh JC, Dohi T, Danial NN, et al. Control of tumor bioenergetics and survival stress signaling by mitochondrial HSP90s. Cancer cell. 2012; 22:331–44. [PubMed: 22975376]

2. Kang BH, Plescia J, Song HY, Meli M, Colombo G, Beebe K, et al. Combinatorial drug design targeting multiple cancer signaling networks controlled by mitochondrial Hsp90. J Clin Invest. 2009; 119:454–64. [PubMed: 19229106]

3. Caino MC, Chae YC, Vaira V, Ferrero S, Nosotti M, Martin NM, et al. Metabolic stress regulates cytoskeletal dynamics and metastasis of cancer cells. J Clin Invest. 2013; 123:2907–20. [PubMed: 23921130]

4. Kang BH, Siegelin MD, Plescia J, Raskett CM, Garlick DS, Dohi T, et al. Preclinical characterization of mitochondria-targeted small molecule hsp90 inhibitors, gamitrinibs, in advanced prostate cancer. Clinical cancer research : an official journal of the American Association for Cancer Research. 2010; 16:4779–88. [PubMed: 20876793]

5. Kang BH, Tavecchio M, Goel HL, Hsieh CC, Garlick DS, Raskett CM, et al. Targeted inhibition of mitochondrial Hsp90 suppresses localised and metastatic prostate cancer growth in a genetic mouse model of disease. British journal of cancer. 2011; 104:629–34. [PubMed: 21285984]

6. Siegelin MD, Dohi T, Raskett CM, Orlowski GM, Powers CM, Gilbert CA, et al. Exploiting the mitochondrial unfolded protein response for cancer therapy in mice and human cells. J Clin Invest. 2011; 121:1349–60. [PubMed: 21364280]

7. Ghosh JC, Siegelin MD, Vaira V, Faversani A, Tavecchio M, Chae YC, et al. Adaptive mitochondrial reprogramming and resistance to PI3K therapy. Journal of the National Cancer Institute. 2015; 107

8. Kang BH, Plescia J, Dohi T, Rosa J, Doxsey SJ, Altieri DC. Regulation of tumor cell mitochondrial homeostasis by an organelle-specific Hsp90 chaperone network. Cell. 2007; 131:257–70. [PubMed: 17956728]

9. Davids MS, Letai A. Targeting the B-cell lymphoma/leukemia 2 family in cancer. Journal of clinical oncology : official journal of the American Society of Clinical Oncology. 2012; 30:3127–35. [PubMed: 22649144]

10. Yip KW, Reed JC. Bcl-2 family proteins and cancer. Oncogene. 2008; 27:6398–406. [PubMed: 18955968]

11. Opferman JT. Attacking cancer's Achilles heel: antagonism of anti-apoptotic BCL-2 family members. FEBS J. 2016; 283:2661–75. [PubMed: 26293580]

12. Karpel-Massler G, Shu C, Chau L, Banu M, Halatsch ME, Westhoff MA, et al. Combined inhibition of Bcl-2/Bcl-xL and Usp9X/Bag3 overcomes apoptotic resistance in glioblastoma in vitro and in vivo. Oncotarget. 2015; 6:14507–21. [PubMed: 26008975]

13. Adams JM, Cory S. The Bcl-2 apoptotic switch in cancer development and therapy. Oncogene. 2007; 26:1324–37. [PubMed: 17322918]

14. Stilgenbauer S, Eichhorst B, Schetelig J, Coutre S, Seymour JF, Munir T, et al. Venetoclax in relapsed or refractory chronic lymphocytic leukaemia with 17p deletion: a multicentre, open-label, phase 2 study. Lancet Oncol. 2016; 17:768–78. [PubMed: 27178240]

15. Souers AJ, Leverson JD, Boghaert ER, Ackler SL, Catron ND, Chen J, et al. ABT-199, a potent and selective BCL-2 inhibitor, achieves antitumor activity while sparing platelets. Nat Med. 2013; 19:202–8. [PubMed: 23291630]

16. Itchaki G, Brown JR. The potential of venetoclax (ABT-199) in chronic lymphocytic leukemia. Ther Adv Hematol. 2016; 7:270–87. [PubMed: 27695617]

17. Sheng Z, Li L, Zhu LJ, Smith TW, Demers A, Ross AH, et al. A genome-wide RNA interference screen reveals an essential CREB3L2-ATF5-MCL1 survival pathway in malignant glioma with therapeutic implications. Nature medicine. 2010; 16:671–7.

18. Karpel-Massler G, Ba M, Shu C, Halatsch ME, Westhoff MA, Bruce JN, et al. TIC10/ONC201 synergizes with Bcl-2/Bcl-xL inhibition in glioblastoma by suppression of Mcl-1 and its binding partners in vitro and in vivo. Oncotarget. 2015; 6:36456–71. [PubMed: 26474387]

19. Karpel-Massler G, Kast RE, Westhoff MA, Dwucet A, Welscher N, Nonnenmacher L, et al. Olanzapine inhibits proliferation, migration and anchorage-independent growth in human glioblastoma cell lines and enhances temozolomide's antiproliferative effect. J Neurooncol. 2015; 122:21–33. [PubMed: 25524815]

20. Karpel-Massler G, Westhoff MA, Zhou S, Nonnenmacher L, Dwucet A, Kast RE, et al. Combined inhibition of HER1/EGFR and RAC1 results in a synergistic antiproliferative effect on established

and primary cultured human glioblastoma cells. Mol Cancer Ther. 2013; 12:1783–95. [PubMed: 23832120]

21. Karpel-Massler G, Westhoff MA, Kast RE, Dwucet A, Nonnenmacher L, Wirtz CR, et al. Artesunate enhances the antiproliferative effect of temozolomide on U87MG and A172 glioblastoma cell lines. Anticancer Agents Med Chem. 2014; 14:313–8. [PubMed: 24506460]
22. Karpel-Massler G, Banu MA, Shu C, Halatsch ME, Westhoff MA, Bruce JN, et al. Inhibition of deubiquitinases primes glioblastoma cells to apoptosis in vitro and in vivo. Oncotarget. 2016; 7:12791–805. [PubMed: 26872380]
23. Karpel-Massler G, Pareja F, Aime P, Shu C, Chau L, Westhoff MA, et al. PARP inhibition restores extrinsic apoptotic sensitivity in glioblastoma. PLoS One. 2014; 9:e114583. [PubMed: 25531448]
24. Karpel-Massler G, Horst BA, Shu C, Chau L, Tsujiuchi T, Bruce JN, et al. A Synthetic Cell-Penetrating Dominant-Negative ATF5 Peptide Exerts Anticancer Activity against a Broad Spectrum of Treatment-Resistant Cancers. Clin Cancer Res. 2016; 22:4698–711. [PubMed: 27126996]
25. Karpel-Massler G, Ramani D, Shu C, Halatsch ME, Westhoff MA, Bruce JN, et al. Metabolic reprogramming of glioblastoma cells by L-asparaginase sensitizes for apoptosis in vitro and in vivo. Oncotarget. 2016; 7:33512–28. [PubMed: 27172899]
26. Pareja F, Macleod D, Shu C, Crary JF, Canoll PD, Ross AH, et al. PI3K and Bcl-2 inhibition primes glioblastoma cells to apoptosis through downregulation of Mcl-1 and Phospho-BAD. Mol Cancer Res. 2014; 12:987–1001. [PubMed: 24757258]
27. Park HK, Lee JE, Lim J, Kang BH. Mitochondrial Hsp90s suppress calcium-mediated stress signals propagating from mitochondria to the ER in cancer cells. Molecular cancer. 2014; 13:148. [PubMed: 24924916]
28. Konopleva M, Contractor R, Tsao T, Samudio I, Ruvolo PP, Kitada S, et al. Mechanisms of apoptosis sensitivity and resistance to the BH3 mimetic ABT-737 in acute myeloid leukemia. Cancer Cell. 2006; 10:375–88. [PubMed: 17097560]
29. Tse C, Shoemaker AR, Adickes J, Anderson MG, Chen J, Jin S, et al. ABT-263: a potent and orally bioavailable Bcl-2 family inhibitor. Cancer research. 2008; 68:3421–8. [PubMed: 18451170]
30. Leverson JD, Phillips DC, Mitten MJ, Boghaert ER, Diaz D, Tahir SK, et al. Exploiting selective BCL-2 family inhibitors to dissect cell survival dependencies and define improved strategies for cancer therapy. Sci Transl Med. 2015; 7:279ra40.
31. Schwickart M, Huang X, Lill JR, Liu J, Ferrando R, French DM, et al. Deubiquitinase USP9X stabilizes MCL1 and promotes tumour cell survival. Nature. 2010; 463:103–7. [PubMed: 20023629]
32. Preuss E, Hugle M, Reimann R, Schlecht M, Fulda S. Pan-mammalian target of rapamycin (mTOR) inhibitor AZD8055 primes rhabdomyosarcoma cells for ABT-737-induced apoptosis by down-regulating Mcl-1 protein. The Journal of biological chemistry. 2013; 288:35287–96. [PubMed: 24133218]
33. Abdulghani J, Gokare P, Gallant JN, Dicker DT, Whitcomb T, Cooper TK, et al. Sorafenib and quinacrine target anti-apoptotic protein Mcl-1: a poor prognostic marker in anaplastic thyroid cancer (ATC). Clin Cancer Res. 2016
34. Dent P. Multi-kinase inhibition in ovarian cancer. Cancer Biol Ther. 2014; 15:1–2. [PubMed: 24309512]
35. Hsu C, Lin LI, Cheng YC, Feng ZR, Shao YY, Cheng AL, et al. Cyclin E1 Inhibition can Overcome Sorafenib Resistance in Hepatocellular Carcinoma Cells Through Mcl-1 Suppression. Clin Cancer Res. 2016; 22:2555–64. [PubMed: 26603262]
36. Rahmani M, Davis EM, Bauer C, Dent P, Grant S. Apoptosis induced by the kinase inhibitor BAY 43–9006 in human leukemia cells involves down-regulation of Mcl-1 through inhibition of translation. J Biol Chem. 2005; 280:35217–27. [PubMed: 16109713]
37. Ricci MS, Kim SH, Ogi K, Plastaras JP, Ling J, Wang W, et al. Reduction of TRAIL-induced Mcl-1 and cIAP2 by c-Myc or sorafenib sensitizes resistant human cancer cells to TRAIL-induced death. Cancer Cell. 2007; 12:66–80. [PubMed: 17613437]

38. Corcoran RB, Cheng KA, Hata AN, Faber AC, Ebi H, Coffee EM, et al. Synthetic lethal interaction of combined BCL-XL and MEK inhibition promotes tumor regressions in KRAS mutant cancer models. Cancer Cell. 2013; 23:121–8. [PubMed: 23245996]

39. Leverson JD, Zhang H, Chen J, Tahir SK, Phillips DC, Xue J, et al. Potent and selective small-molecule MCL-1 inhibitors demonstrate on-target cancer cell killing activity as single agents and in combination with ABT-263 (navitoclax). Cell Death Dis. 2015; 6:e1590. [PubMed: 25590800]

40. Chae YC, Angelin A, Lisanti S, Kossenkov AV, Speicher KD, Wang H, et al. Landscape of the mitochondrial Hsp90 metabolome in tumours. Nat Commun. 2013; 4:2139. [PubMed: 23842546]

41. Allen JE, Krigsfeld G, Mayes PA, Patel L, Dicker DT, Patel AS, et al. Dual inactivation of Akt and ERK by TIC10 signals Foxo3a nuclear translocation, TRAIL gene induction, and potent antitumor effects. Science translational medicine. 2013; 5:171ra17.

42. Perciavalle RM, Stewart DP, Koss B, Lynch J, Milasta S, Bathina M, et al. Anti-apoptotic MCL-1 localizes to the mitochondrial matrix and couples mitochondrial fusion to respiration. Nat Cell Biol. 2012; 14:575–83. [PubMed: 22544066]

43. Ye J, Kumanova M, Hart LS, Sloane K, Zhang H, De Panis DN, et al. The GCN2-ATF4 pathway is critical for tumour cell survival and proliferation in response to nutrient deprivation. The EMBO journal. 2010; 29:2082–96. [PubMed: 20473272]

44. Ramirez-Peinado S, Alcazar-Limones F, Lagares-Tena L, El Mjiyad N, Caro-Maldonado A, Tirado OM, et al. 2-deoxyglucose induces Noxa-dependent apoptosis in alveolar rhabdomyosarcoma. Cancer Res. 2011; 71:6796–806. [PubMed: 21911456]

45. Wang Q, Mora-Jensen H, Weniger MA, Perez-Galan P, Wolford C, Hai T, et al. ERAD inhibitors integrate ER stress with an epigenetic mechanism to activate BH3-only protein NOXA in cancer cells. Proc Natl Acad Sci U S A. 2009; 106:2200–5. [PubMed: 19164757]

46. Yan J, Zhong N, Liu G, Chen K, Liu X, Su L, et al. Usp9x- and Noxa-mediated Mcl-1 downregulation contributes to pemetrexed-induced apoptosis in human non-small-cell lung cancer cells. Cell death & disease. 2014; 5:e1316. [PubMed: 24991768]

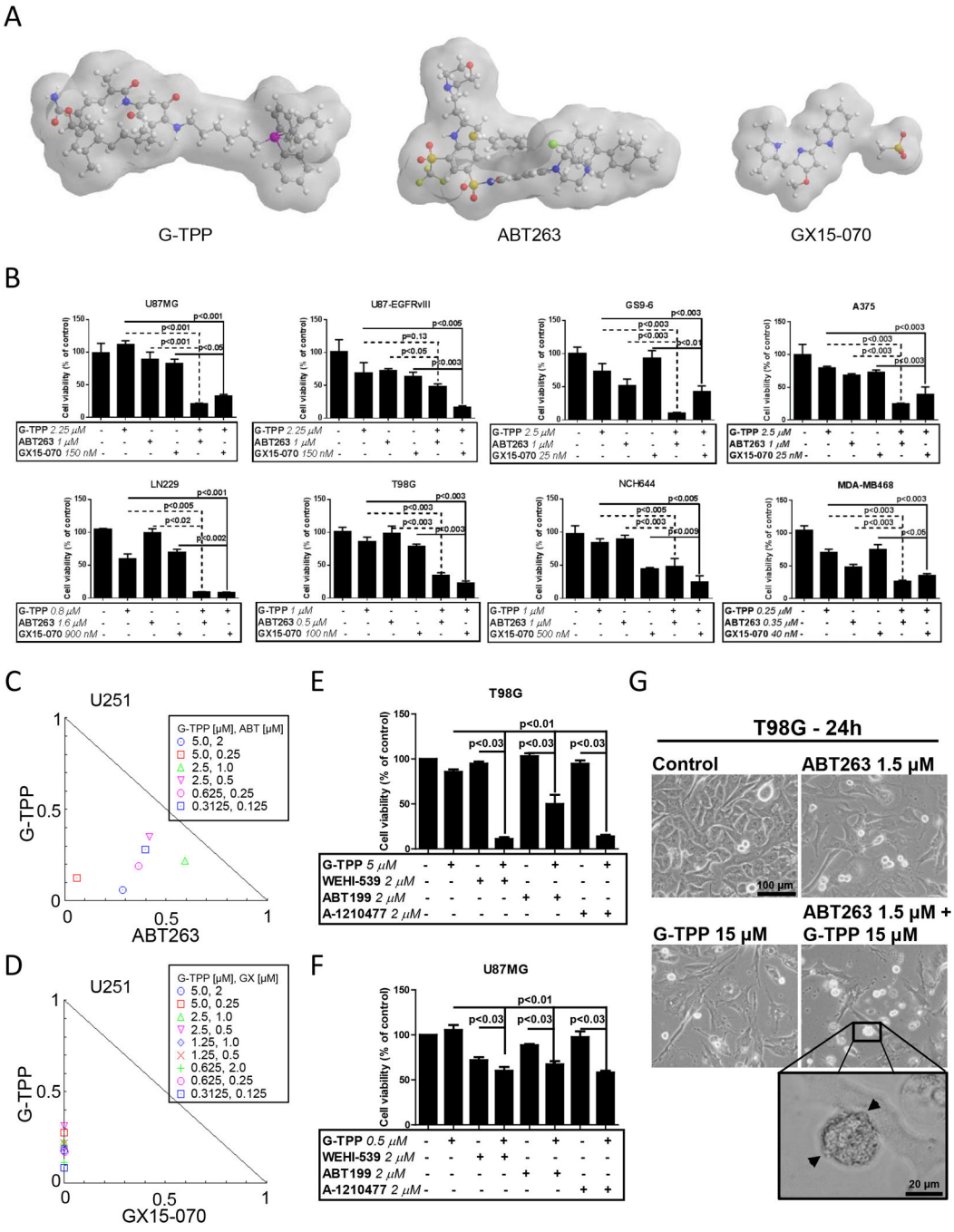

Figure 1.

Combined treatment with BH3-mimetics (ABT263, GX15-070) and the mitochondrial matrix inhibitor Gamitrinib (G-TPP) results in a synergistic antiproliferative effect across a wide spectrum of human glioma and other solid cancer cells. A, 3-dimensional representation of the chemical structures of G-TPP, ABT263 and GX15-070. B, U87MG, U87-EGFRvIII, LN229, T98G established glioblastoma cell lines, GS9-6 and NCH644 glioma stem-like cells, A375 melanoma and MDA-MB-468 breast cancer cells were treated as indicated with G-TPP, ABT263, GX15-070 or the respective drug combinations under

serum starvation (1.5% FBS). After 72h of treatment, MTT assays were performed. Column: mean. Error bar: standard error of the mean (SEM). Statistical analysis was performed and p-values were calculated. C–D, U251 glioblastoma cells were treated for 72 hours with ABT263 (C), GX15-070 (D), G-TPP or the combination as indicated. Normalized isobolograms were calculated using the CompuSyn software (ComboSyn, Inc., Paramus, NJ, U.S.A.). Data points located on the line indicate an additive drug-drug interaction. Data points located below the line indicate a synergistic drug-drug interaction and data points above the line indicate an antagonistic drug-drug interaction. E–F, T98G and U87MG cells were treated as indicated with G-TPP, WEHI-539, ABT199, A-1210477 or the respective drug combinations under serum starvation (1.5% FBS). After 72h of treatment, CellTiter Glo® assays were performed. Column: mean. Error bar: standard deviation (SD). Statistical analysis was performed and p-values were calculated. G, Representative microphotographs of T98G glioblastoma cells after 24 h of treatment with G-TPP, ABT263 or both. Morphological changes such as a rounding of cells and the formation of blebs (arrowheads) are commonly seen after treatment with both agents.

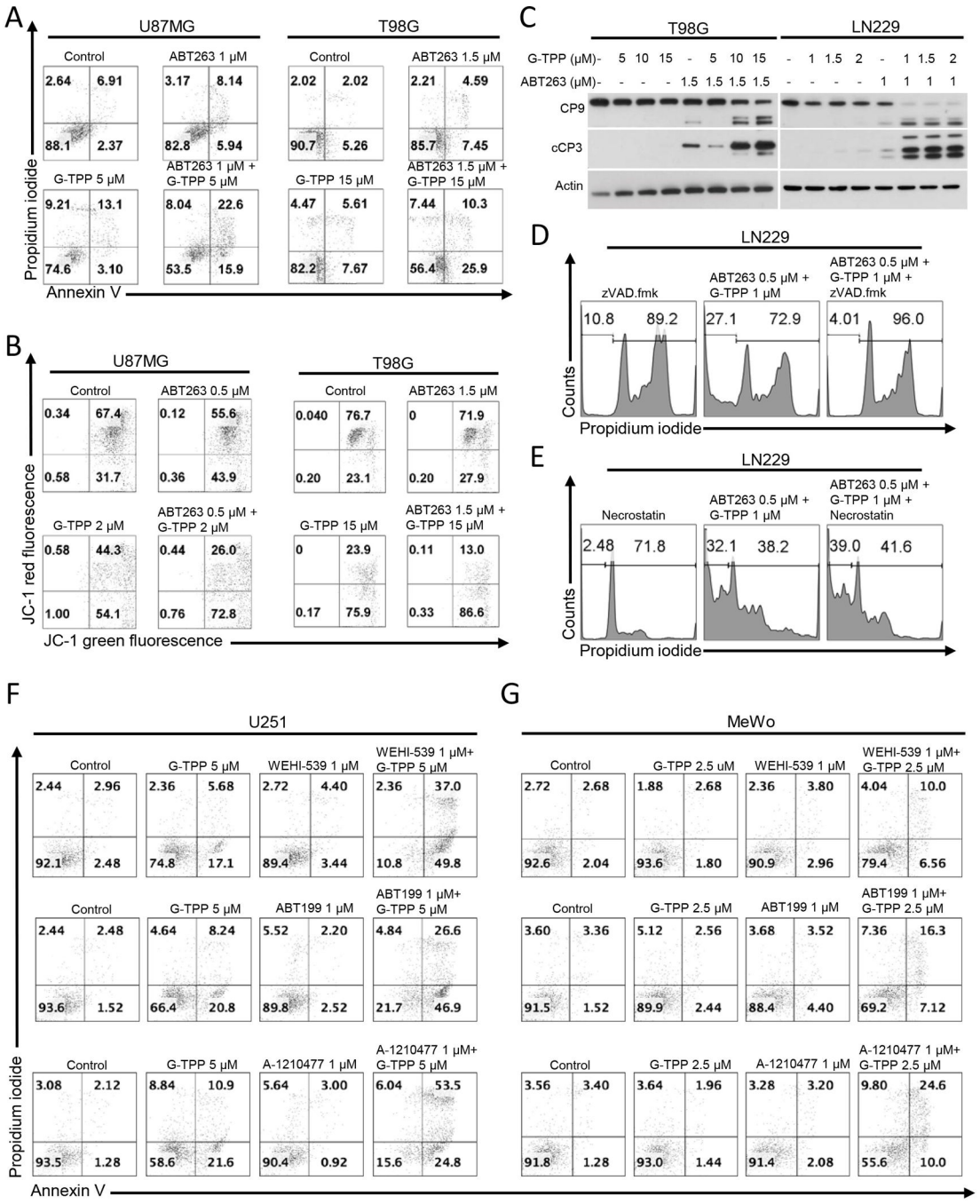

Figure 2.

Combined treatment with G-TPP and broad or selective BH3-mimetics yields enhanced induction of apoptosis. A, Representative histograms of U87MG and T98G glioblastoma cells treated with solvent, ABT263, G-TPP or the combination as indicated for 48h prior to staining for Annexin V and propidium iodide and flowcytometric analysis. B, Representative histograms of U87MG and T98G glioblastoma cells that were treated for 24 h with G-TPP, ABT263, both or solvent prior to staining with JC-1 and flow cytometric analysis. C, T98G and LN229 glioblastoma cells were treated for 7 h with G-TPP, ABT263, both agents and

solvent under serum starvation. Whole-cell extracts were examined by Western blot analysis for caspase 9 (CP9) and cleaved caspase 3 (cCP3). Actin Western blot analysis was performed to confirm equal protein loading. D, LN229 cells were treated with the combination of ABT263 and G-TPP as indicated in the presence or absence of the pan-caspase inhibitor zVAD.fmk (20μM). Staining for propidium iodide and flowcytometric analysis was performed to determine the fraction of subG1 cells. E, LN229 cells were treated with the combination of ABT263 and G-TPP as indicated in the presence or absence of necrostatin (20μM). Staining for propidium iodide and flowcytometric analysis was performed to determine the fraction of subG1 cells. F–G, U251 glioblastoma (F) or MeWo melanoma (G) cells were treated with selective BH-3 mimetics, G-TPP or the combination of both for 24 h (U251) or 48 h (MeWo). Thereafter, cells were stained with annexin V and propidium iodide and analyzed by flow cytometry. Shown are representative flow plots.

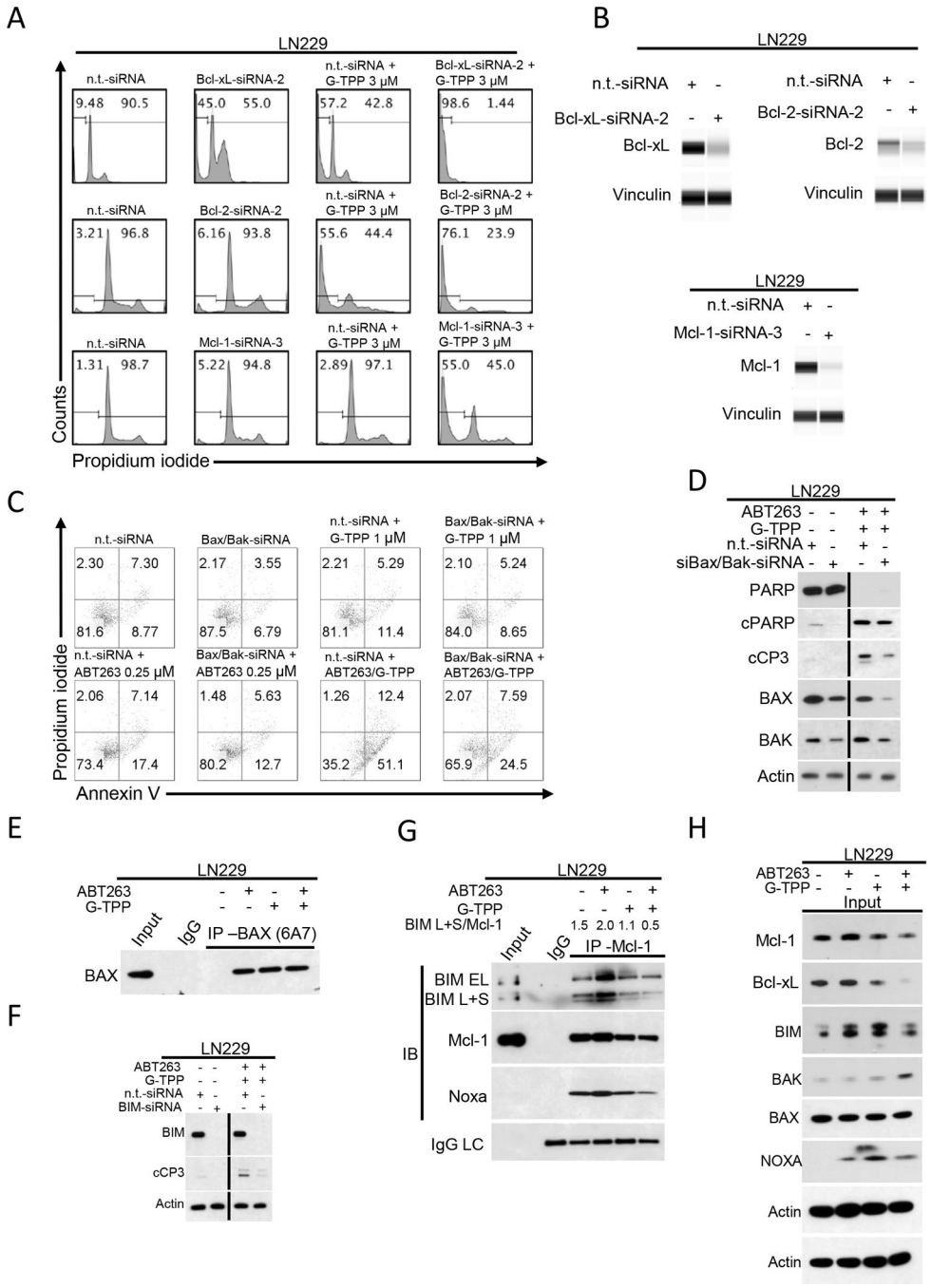

Figure 3.

Knockdown of Bcl-xL, Bcl-2 and Mcl-1 sensitizes for G-TPP-mediated apoptosis. A, Representative flow plots of LN229 cells that were treated with n.t.-siRNA, Bcl-xL-, Bcl-2- or Mcl-1-siRNAs prior to additional treatment with either solvent or G-TPP. Staining for propidium iodide and flowcytometric analysis was performed to determine the fraction of subG1 cells. B, Knockdown of Bcl-xL, Bcl-2 and Mcl-1 was confirmed by capillary electrophoresis. Vinculin served as loading control. C, LN229 cells were treated with n.t.-siRNA or Bax/Bak-siRNA prior to treatment with solvent, ABT263, G-TPP or the

combination as indicated. Staining for Annexin V and propidium iodide was performed prior to flowcytometric analysis. Representative flow plots are shown. Bax/Bak knockdown was confirmed by Western blot analysis (see figure 3D). D, Whole cell extracts were collected from LN229 cells treated with n.t.-siRNA or Bax/Bak-siRNA in the presence or absence of 0.25μM ABT263/1μM G-TPP followed by Western blot analysis for PARP, cPARP, cCP3, BAX and BAK. Equal loading was verified by Western blot analysis for Actin. E, LN229 cells were treated with solvent, 0.25μM ABT263, 1μM G-TPP or the combination. Immunoprecipitation (IP) for BAX (6A7) was performed prior to immunoblotting for Bax. IP with non-specific IgG was used as a negative control. F, LN229 cells were treated with n.t.-siRNA or BIM-siRNA in the presence or absence of 0.25μM ABT263/1μM G-TPP. Whole cell extracts were collected and Western blot analysis was performed for BIM and cCP3. Actin served as a loading control. G, LN229 cells were treated with solvent, 0.25μM ABT263, 1μM G-TPP or the combination. Whole cell extracts were collected prior to co-immunoprecipitation for Mcl-1. Immunoblots for Bim, Mcl1, Noxa and the IgG light chain (LC) were performed. The BIM L+S/Mcl-1 ratio was calculated based on densitometric analysis using ImageJ 1.47v (http://imagej.nih.gov/ij). H, Western blot analysis for Mcl-1, Bcl-xL, BIM, Bak, Bax and Noxa of LN229 cells treated as described for G. Actin served as loading control.

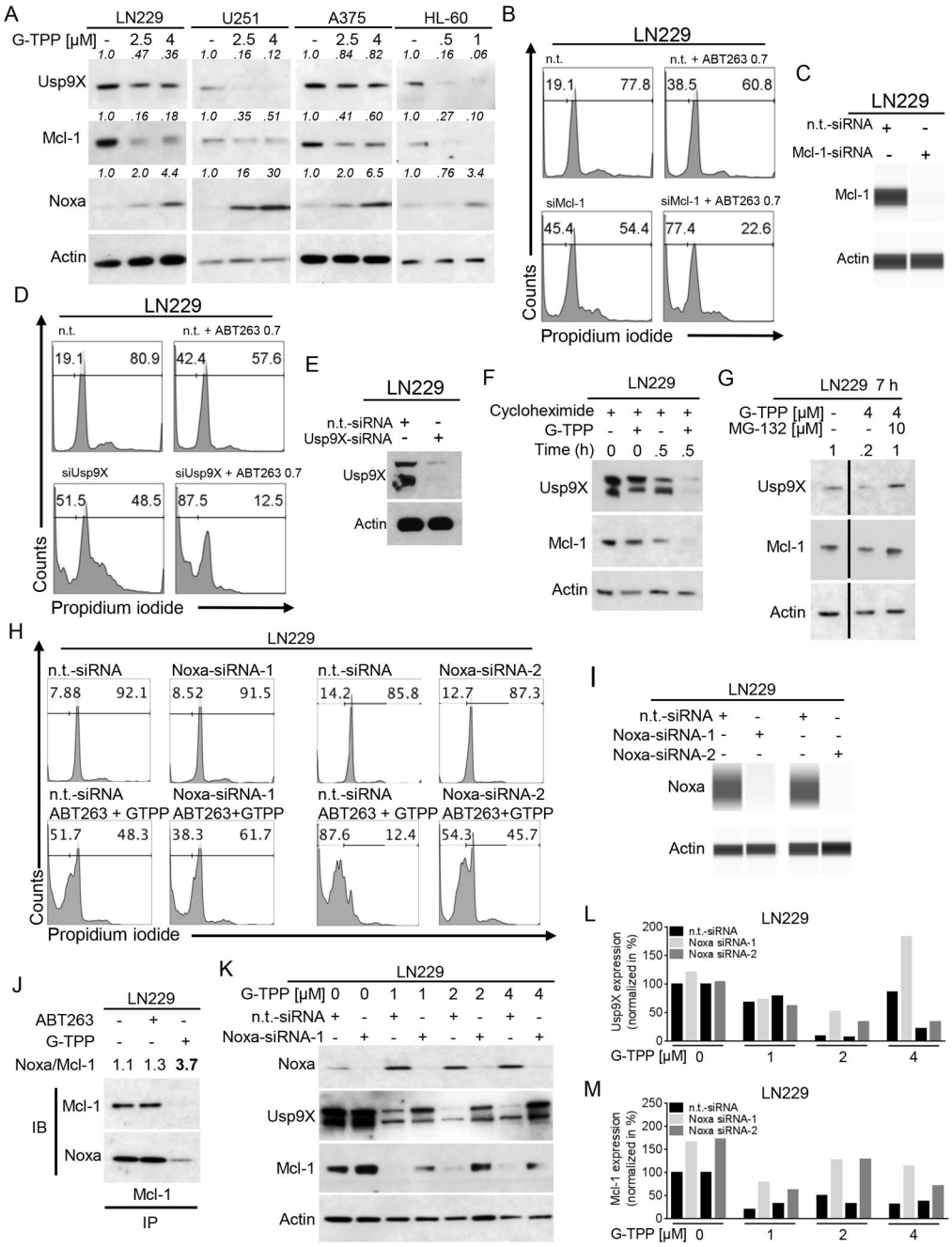

Figure 4.

Treatment with G-TPP increases the Noxa/Mcl-1 ratio. A, LN229 and U251 glioma, A375 melanoma and HL-60 acute promyelocytic leukemia cells were treated with increasing concentrations of G-TPP as indicated. Whole cell extracts were collected and Western blot analysis was performed for Usp9X, Mcl-1 and Noxa. Actin served as loading control. Western blots were quantified. B, LN229 cells were treated with ABT263 in the presence or absence of siRNA-mediated Mcl-1 knockdown prior to staining for propidium iodide and flow cytometric analysis. Representative flow plots are shown displaying the fraction of

subG1 cells. C, LN229 cells were treated as described for B. Capillary electrophoresis for Mcl-1 was performed. D, LN229 cells were treated with ABT263 in the presence or absence of siRNA-mediated Usp9X knockdown prior to staining for propidium iodide and flow cytometric analysis. Representative flow plots are shown displaying the fraction of subG1 cells. E, LN229 cells were treated as described for D. Western blot analysis for Usp9X was performed. F, LN229 cells were treated with solvent or G-TPP for 0h or 0.5h in the presence of 10μg/ml cycloheximide. Western blot analysis was performed for Usp9X and Mcl-1. Actin Western blot analysis served as a loading control. G, LN229 cells were treated for 7h with solvent or G-TPP in the presence or absence of 10μM MG-132. Western blot analysis was performed for Usp9X and Mcl-1. Actin Western blot analysis served as a loading control. H, LN229 cells were treated with n.t.-siRNA or 2 different Noxa-siRNAs in the presence or absence of 0.25μM ABT263/1μM G-TPP. Staining for propidium iodide and flowcytometric analysis was performed to determine the fraction of subG1 cells. Representative flow plots are shown. I, LN229 cells were treated as described for H. Capillary electrophoresis was performed to confirm Noxa knockdown. J, LN229 cells were treated for 24h with solvent, 1μM ABT263 or 5μM G-TPP prior to collection of whole cell extracts. Co-immunoprecipitation for Mcl-1 was performed prior to immunoblotting for Mcl-1 and Noxa. The Noxa/Mcl-1 ratio was calculated based on densitometric analysis. K, LN229 cells were treated with n.t.-siRNA or Noxa-siRNA1 in the absence or presence of G-TPP as indicated. Whole cell extracts were collected prior to Western blot analysis for Noxa, Usp9X or Mcl-1. Actin Western blot was performed to control for loading. L–M, Quantitative representation of LN229 cells treated as described for K. Densitometric analysis was performed normalizing the Usp9X (L) or Mcl-1 (M) signal to the respective Actin control.

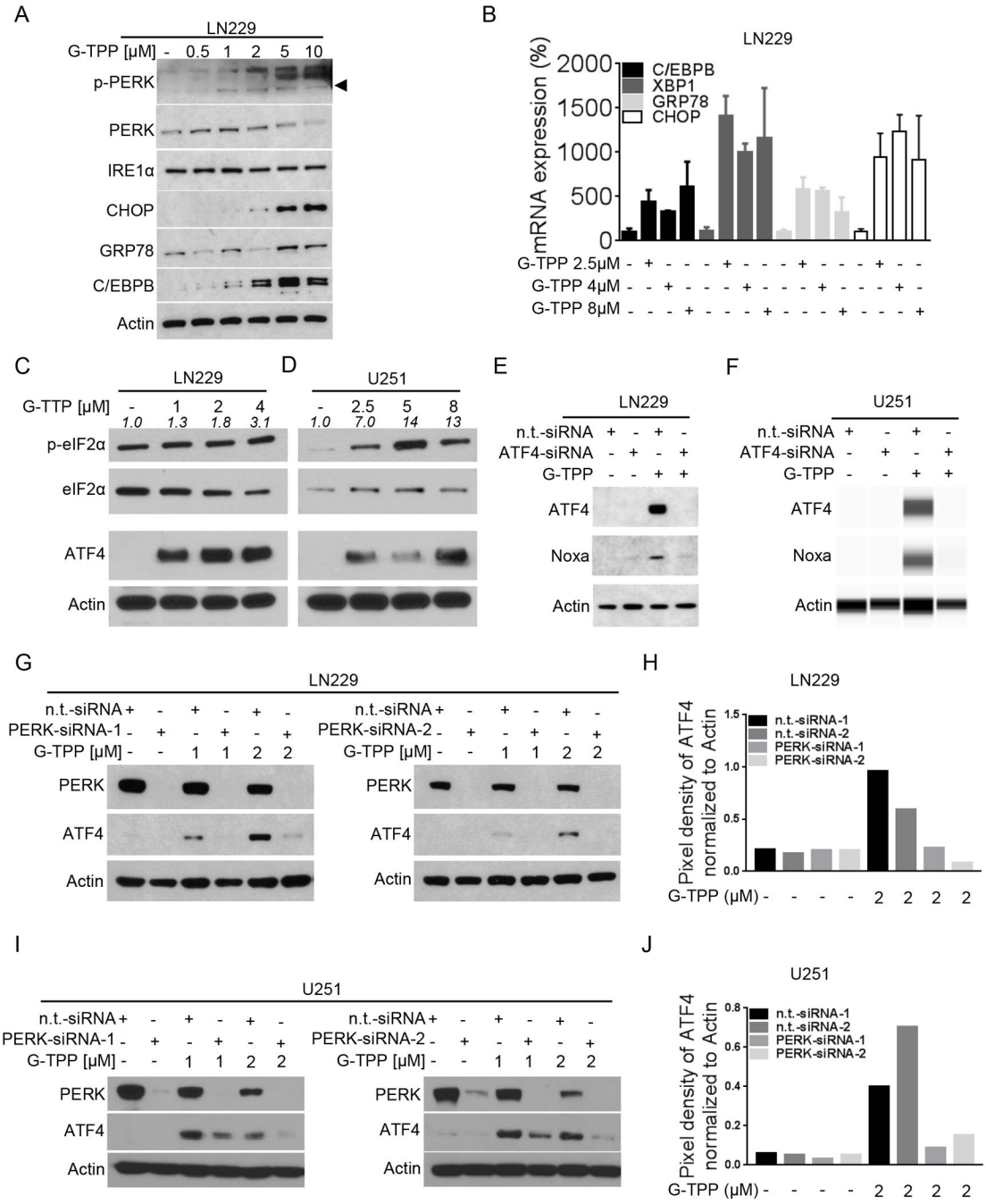

Figure 5.

Treatment with G-TPP elicits an ER-stress response. A, LN229 cells were treated with increasing concentrations of G-TPP for 7h. Western blot analysis was performed for p-PERK, PERK, IRE1α, CHOP, GRP78 and C/EBPB. Western blot for Actin served as loading control. B, LN229 cells were treated with increasing concentrations of G-TPP for 7h. Total RNA was collected and real-time rtPCR was performed for C/EBPB, XBP1, GRP78 and CHOP. Column: mean. Error bars: SD. C–D, LN229 (C) and U251 (D) cells were treated with increasing concentrations of G-TPP for 7h. Whole cell extracts were

collected prior to Western blot analysis for p-eIF2α, eIF2α and ATF4. Equal loading was controlled by Actin Western blot. Densitometric analysis of p-eIF2α in relation to eIF2α was performed. E-F, LN229 (E) and U251 (F) cells were treated with n.t.-siRNA or ATF4-siRNA in the presence or absence of 2μM G-TPP. Whole cell extracts were collected prior to Western blot analysis or capillary electrophoresis for ATF4 and Noxa. Actin served as loading control. G-I, LN229 (G) cells and U251 (I) cells were incubated with n.t.-siRNA or 2 different PERK-siRNAs prior to treatment with solvent or G-TPP as indicated. Western blot analysis was performed for PERK and ATF4. Western blot for Actin served to control for equal loading. H–J, Quantitative representation of ATF4 expression for LN229/U251 cells treated as described for G and I. Densitometric analysis was performed.

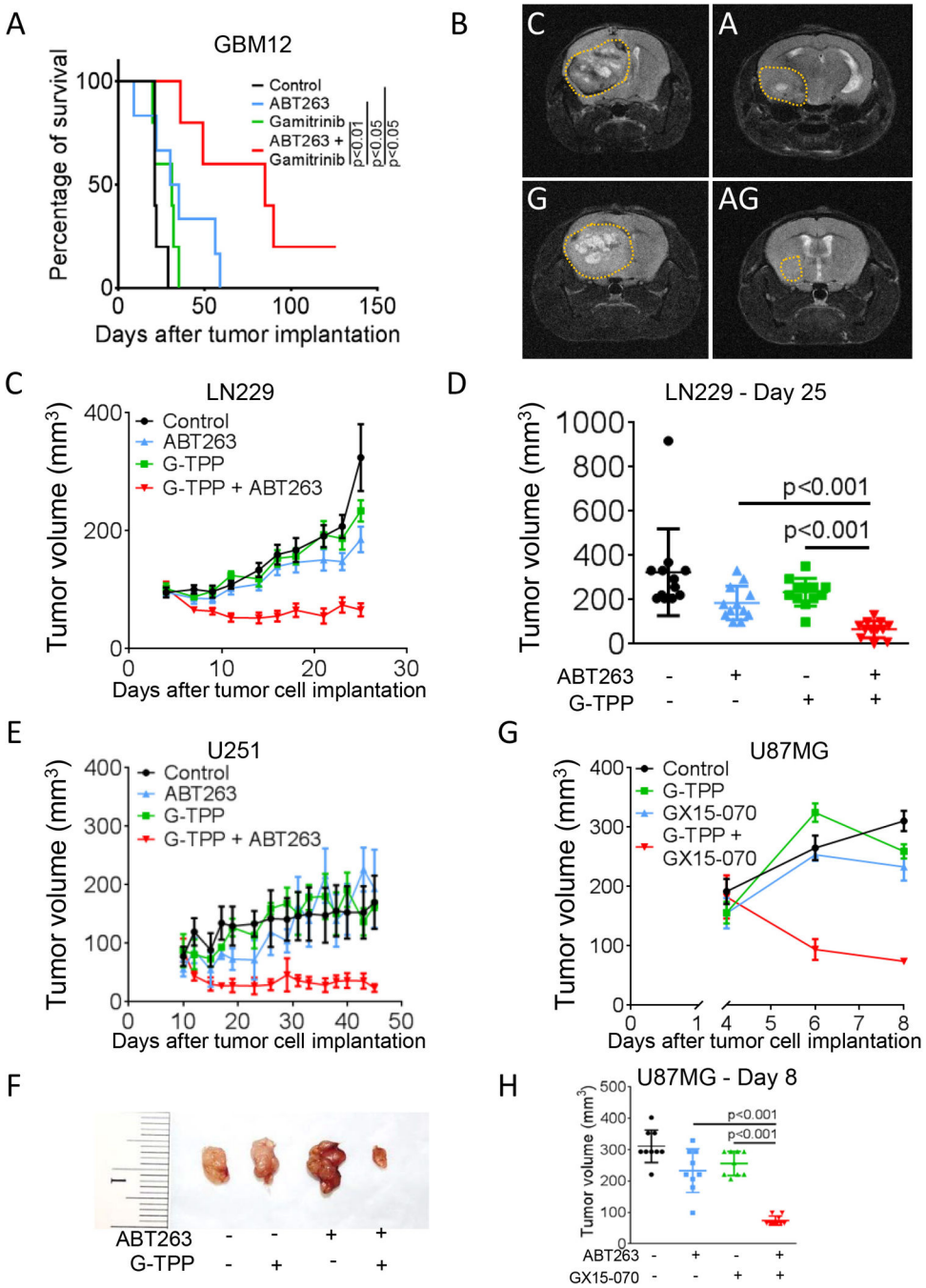

Figure 6.

Combined treatment with ABT263 and G-TPP prolongs survival in glioma models in vivo. A, 3×10^5 GBM12 cells were implanted into the right striatum of nude mice. Once tumors formed animals were randomized and treated subcutaneously 3×/week with vehicle (n=5), ABT263 25mg/kg (n=6), G-TPP 5mg/kg (n=5) or the combination (n=5). Kaplan-Meier plots were calculated for analysis of survival. Animals treated with ABT263+Gamitrinib-TPP had a significantly longer overall survival than animals receiving, vehicle, ABT263 or Gamitrinib-TPP ($p<0.05$, log-rank (Mantel-Cox) test). B, Representative MRI images of

animals treated as described for A towards the end of the experiment. C=vehicle, A=ABT263, G=G-TPP, AG=ABT263 plus G-TPP. C–F, 1×10^6 LN229 (C–D) and U251 (E–F) glioblastoma cells were implanted subcutaneously. After tumor formation animals were treated intraperitoneally with vehicle, G-TPP (5 mg/kg), ABT263 (50 mg/kg) or both agents. Data are presented as mean and SEM. Tumor growth curves show the development of tumor size for each treatment group. Scatter plots display the quantitative representation of the tumor size among the different treatments toward the end of the experiments. A Photograph of representative tumors is shown for U251 (F). G–H, 1×10^6 U87MG glioblastoma cells were implanted subcutaneously. After tumor formation animals were treated intraperitoneally with vehicle, G-TPP (5 mg/kg), GX15-070 (5 mg/kg) or both agents. Data are presented as mean and SEM. Tumor growth curves show the development of tumor size for each treatment group (G). Scatter plots display the quantitative representation of the tumor size among the different treatments toward the end of the experiments (H).

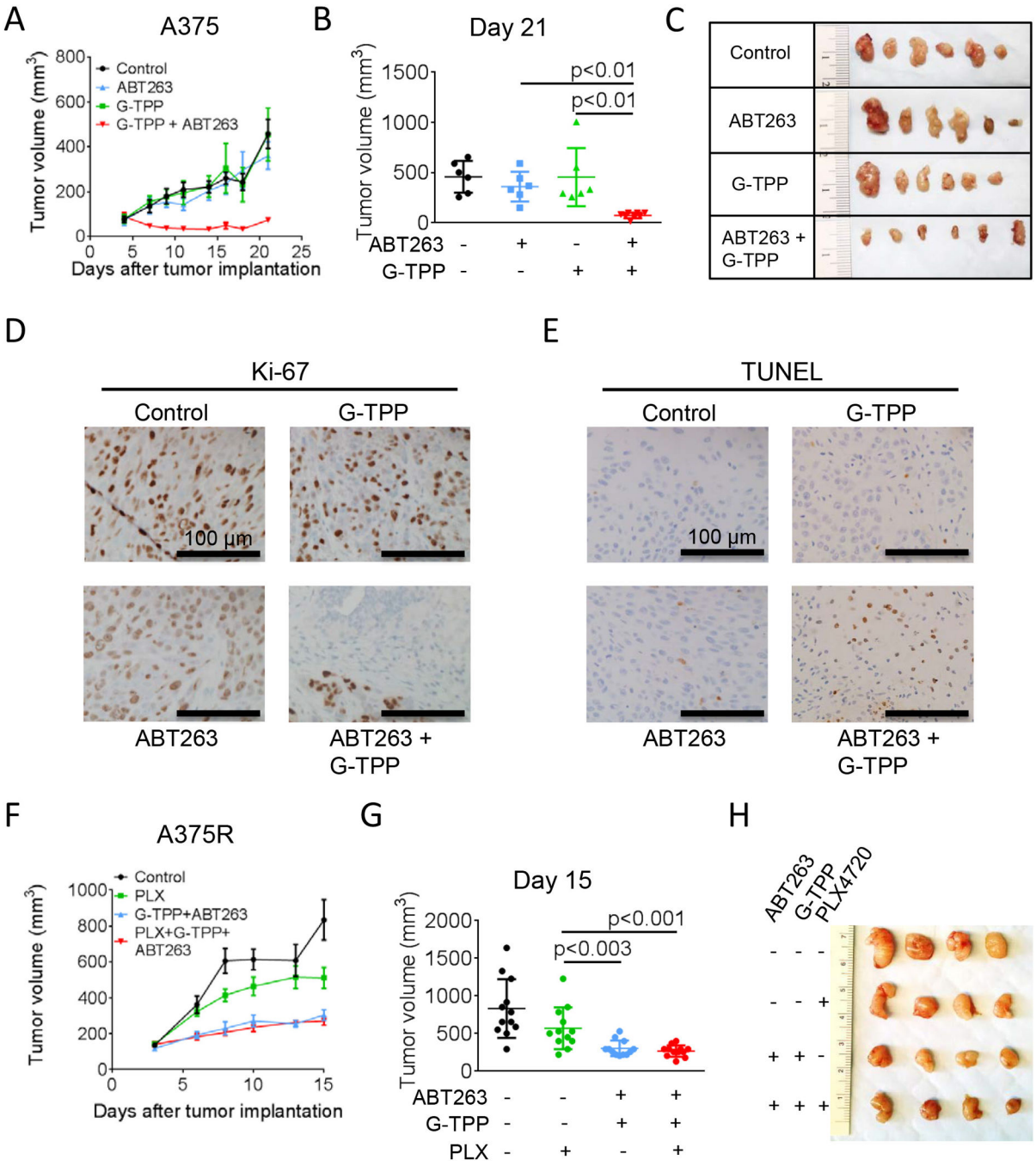

Figure 7.

Combined treatment with ABT263 and G-TPP reduces the tumor growth rate of B-RafV600E inhibitor responsive and resistant melanomas in vivo. A, 1×10^6 A375 melanoma cells were implanted subcutaneously into nude mice. After tumor formation animals were treated intraperitoneally with vehicle, G-TPP (5 mg/kg), ABT263 (50 mg/kg) or both agents. Data are presented as mean and SEM. Tumor growth curves show the development of tumor size for each treatment group. B, Scatter plots display the quantitative representation of the tumor size among the different treatments toward the end of the experiment (day 21). C,

Photographs of representative tumors explanted from mice treated as described for A. D, Representative microphotographs of tissue sections stained for Ki-67. Magnification, 20×. E, Representative microphotographs of tissue sections subjected to TUNEL staining. Magnification, 20×. F, 1×10^6 B-RafV600E inhibitor (PLX-4720)-resistant A375R melanoma cells were treated intraperitoneally with vehicle, PLX-4720 (25 mg/kg), G-TPP (5 mg/kg) plus ABT263 (50 mg/kg) or all three agents. Data are presented as mean and SEM. Tumor growth curves show the development of tumor size for each treatment group. G, Scatter plots display the quantitative representation of the tumor size among the different treatments toward the end of the experiment (day 15). H, Photographs of representative tumors explanted from mice treated as described for F